An Intelligent System for Early Detection and Diagnosis of Diabetic Retinopathy based on Statistical and Radon Transform Features of Retina Images

Dr. Raghad Z. Yousif **Dr. Nabeel George Nacy**
Dr. Ramzi Raphael Barwari
college of Science **College of Administration and Economics**
College of Engineering
Raghad.yousif@su.edu.krd **ngnacy_54@yahoo.com**
ramziraphael@gmail.com
Salahaddin University-Kurdistan Region-Iraq

Abstract :

The eye is one of the most important end organs for complications of diabetes. There are two types of ocular diabetic complications: direct and indirect. Diabetic retinopathy is the primary direct complication of diabetes in the eye. There are two main categories of DR, Non-proliferative (Non-PDR) and Proliferative (PDR). In this work a new technique is presented for automatic screening of diabetic Retinopathy based on Comprehensive Spectral-Textural features which are two fundamental patterns elements that can be interpreted by human. To extract spectral features parameters (Bi-spectral invariant features at different angles of orientation) the gray level retina images are subjected to Radon transform which convert the 2D image in to 1D image vector which introduced to the HOS (Higher Order Statistic) Scheme. Nineteen Textural features parameter were derived from gray level matrix, co-occurrence matrix, and run length matrix features to perform texture analysis for retina images and hence to generate the features vector. Later twenty-six best features form both categories (spectral & Textural) have been considered and introduced to the features selection stage to exclude irrelevant features. Thus a feature vector is reduced to 10- relevant features for each retina image. The database used is in this work is MESSADOR, with 150 retinal images have been used for training and validation stages .Two classifiers were presented , K-Nearest-Neighbor (KNN) and Naïve Bayes Neural Network with different rates. The simulation results show that the proposed system can attain very high Performance (Accuracy) about 98.09%.

Keywords: CAD, Diabetic retinopathy, Radon transform, Spectral-Textural Features, KNN.

نظام ذكي للكشف المبكر والتشخيص لاعتلال الشبكية نتيجة السكري بناءً على المميزات الإحصائية و المميزات الطيفية من تحويل رادون لصور شبكية العين

أ.م. د. رغد زهير يوسف كلية العلوم
أ.م. د. نبيل جورج ناسي كلية الأدارة والأقتصاد
أ.م.د. رمزي روفائيل برواري كلية الهندسة
جامعة صلاح الدين – اقليم كردستان – العراق
raghad.yousif@su.edu.krd

المستخلص:

يعتبر اعتلال الشبكية السكري أهم المضاعفات المباشرة الأولية لمرض السكري في العين. هناك فئتان رئيسيتان من DR ، غير التكاثري (non- PDR) و التكاثري (PDR) . في هذا البحث ، تم تقديم تقنية جديدة للفحص التلقائي لاعتلال الشبكية السكري بناءً على ميزات طيفية نصية شاملة ، وهما عنصران أساسيان في النموذج يمكن تفسيرهما من قبل الإنسان. لاستخراج معلمات الميزات الطيفية (ميزات الثنائي الطيفي في زوايا مختلفة من الاتجاه) ، تتعرض صور شبكية العين ذات المستوى الرمادي لتحويل Radon الذي يحول الصورة ثنائية الأبعاد إلى متجه صورة D1 والذي تم تقديمه إلى مخطط HOS (إحصائيات الترتيب العالي). بينما تم اشتقاق معلمة ميزات Textural التسعة عشر من مصفوفة المستوى الرمادي ، مصفوفة الحدوث المشتركة ، وميزات طول مصفوفة التشغيل مجتمعة لإجراء تحليل نسيج لصور شبكية العين ، وبالتالي لتوليد متجه الميزات. بعد ستة وعشرين أفضل ميزة تم تشكيل كلتا الفئتين وتم إدخالهما في مرحلة اختيار الميزات لتقليل متجه المعالم إلى 10 ميزات لكل صورة لشبكية العين. قاعدة البيانات المستخدمة في هذا العمل هي MESSADOR ، وبالتالي تم استخدام أكثر من 150 صورة شبكية للتدريب واختبار اثنين من المصنفات المقدمة على أساس K-Nearest-Neighbour (KNN) و Naïve Bayes Neural Network بمعدلات مختلفة. اظهرت نتائج المحاكاة أن النظام المقترح يمكن أن يحقق معدلات تصنيف عالية جدًا تبلغ حوالي 98.09٪.

الكلمات الرئيسية: CAD ، اعتلال الشبكية السكري ، تحويل الرادون ، الميزات الطيفية النصية ، KNN.

I. INTRODUCTION

Automatic screening of DR used by the doctors as a second aim for detection and identification the stages of this disease with more accurate and precise ways. DR is one of the most prevalent worldwide diseases that leading cause of blindness due to the damage blood vessels in the eye from elevated blood sugar [1]. It can be treated if the diagnosis shows that patient with diabetes that holds early signs of retinopathy otherwise it will be ended with a complete loss of vision. The most common form of DR can be classified onto two stages; Non-proliferative and Proliferative [2]. The main symptoms are usually observed in Non-PDR stage; micro aneurysm dots, hemorrhages, cotton and wool spots, hard exudate, loops, venous bleeding, and Capillary leakage causes Diabetic Macular Edema (DME). Early diagnosis in Non-proliferative can prevents vision loss in human beings. In contrast, Proliferative is the most advanced stage. It occurs Automatic screening of diabetic Retinopathy helps doctors to quickly identify the condition of the patient with more accurate way. Diabetic Retinopathy (DR) is asymptomatic till it becomes vision – threating. If left undiagnosed at the initial stage it can lead to partial or even complete loss of visual capacity, Retinal lesions associated with diabetes are used to evaluate different stages. The main two stages of (DR) are called non-Proliferative and Proliferative [3]. Figure (1) shows a comparison between the symptoms Non-PDR and PDR. The non-Proliferative is the earliest form where several changes of early retinopathy are seen including microaneurysms dots and some hemorrhage, cotton and wool spots, hard exudate, loops, venous bleeding and intra retinal microvascular abnormality (IRMA). These changes are mostly seen in the background and do not results in visual loss. The PDR on other hand is characterized by the proliferation of abnormal new vessels either on the disk called neovascularization on the disk (NVD) or else where the surface of retina called neovascularization elsewhere (NVE)[2][4]. Both the forms have tendency to bleed resulting in sever visual losses and thus need urgent attention for laser photocoagulation. The new vessels are combined with fibrosis resulting in the formation of fibrovascular tissue. While growing along the posterior hyaloid these leaky vessels leads to localized liquefaction of the vitreous gel. Localized collapse of vitreous gel causes vitreous contraction resulting in rupture of these fragile vessels causing vitreous hemorrhage [5]. Thus Medical imaging allows scientists and physicians to understand potential life-saving information using less invasive techniques. This automated algorithm indicates places in the image that require extra attention from the physician because they could be abnormal. These technologies are called Computer Aided Diagnosis (CAD). This paper describes components of an automatic system that can aid in the detection of

diabetic retinopathy. As the number of diabetes affected people is increasing worldwide, the need for automated detection methods of diabetic retinopathy will increase as well. To automatically detect diabetic retinopathy, a computer has to interpret and analyze digital images of the retina.

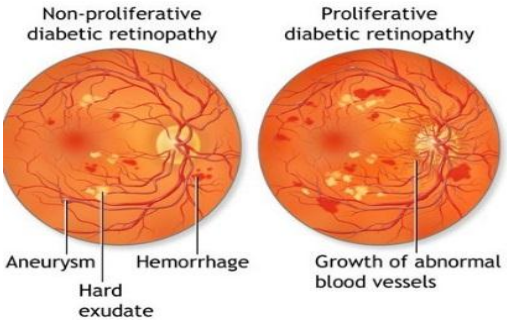

Fig1. Symptoms of Non-PDR and PDR on retina image

Extraction of, the Spectral features using Radon transform and, gray level co-occurrence matrix based Textural features from color fundus images are used. Some of related work accuracy of this work is presented by Bazhdar N. SH. Mohammed, et al [4] used Neutrosophic set (NS) domain based on statistical features, Gray Level Co-occurrence Matrix (GLCM), Gray Level Run Length Matrix (GLRLM), and difference statistics for features extraction of diabetic retinopathy. More than thirty statistical textural features derived from the NS set domain and spatial domain have been tested using a features selection scheme named one-way analysis of variables (ANOVA1) with significance value ($p < 0.001$) .Giri Babu Kande [6] which propose a method of polynomial contrast enhancement and dark lesion detection based on Mathematical Morphology. In this method Morphological top-hat transformation is used to segment candidate MAs from blood vessels. A.M. Mendonça et al. [7] used mean filter to the original image, obtaining a normalized image and scaling as preprocessing techniques. To discriminate microaneurysms from blood vessels "top-hat" transform and a Gaussian shaped matched filter is used. Abhir Bhalerao et al. [8] used median filter for contrast normalization and contrast enhancement as preprocessing techniques. Orientation matched filter was used to differentiate microaneurysms from blood vessels. Thresholding on the output of orientation matched filter is done to obtain a set of potential candidates (MAs). Eigen image analysis applied to the potential candidate regions and a second threshold applied on the Eigen-space projection of the candidate regions eliminated certain noise artifacts. Iqbal, M.I et al. [9] used Color Space Conversion, Edge Zero Padding, Median Filtering and Adaptive Histogram Equalization as pre-processing techniques and they used segmentation to group the image into regions with same property or characteristics. Methods of image segmentation include simple thresholding, K-means Algorithm and Fuzzy

C-means. Akara Sopharak et al. [10] used median filtering, contrast enhancement by Contrast Limited Adaptive Histogram Equalization and shade correction as pre-processing steps and he used Extended-minima transform for feature extraction. Priya R et al. [11] used pre-processing techniques like Gray Scale Conversion, Adaptive Histogram Equalization, Matched Filter Response and proposed a method for feature extraction based on Area of on pixels, Mean and Standard Deviation. S. Saranya et al[12] use Eigenvalues from hessian matrix in detection of diabetic retinopathy. Vijay M Mane etal, [13] this paper presents a unique methodology for automatic detection of red lesions in fundus images. Proposed methodology employs modified approach to matched filtering for extraction of retinal vasculature and detection of candidate lesions. Features of all candidate lesions are extracted and are used to train Support Vector Machine classifier. The next section will describe the proposed system methodology.

II. Proposed System Methodology

The framework for the proposed methodology is given in Figure 2. The input retinal images undergo preprocessing which involves image resize followed by image Denoising using median filter then image enhancements with powerful proposed Technique based on Laplacian pyramid. Then after the output from preprocessing block is introduce to both radon transform systems which is start by theta selection followed by applying Radon transform before spectral features extraction using HOS (Higher order statistics technique) Scheme. The Textural features involve a features derived from Texture analysis tools, GLCM (Gray Level Co-occurrence Matrix) and run length matrix. These features were combined with spectral features to feature vector. The initial feature vector contains basically 26 features introduced to feature selection stage which aimed to select the top 10 features from both groups. These features then will be used for training two types of classifiers (KNN and Bayes Naïve) to classify the category of retina images (normal or abnormal (PDR ,or Non-PDR)) based on the presence of DR.

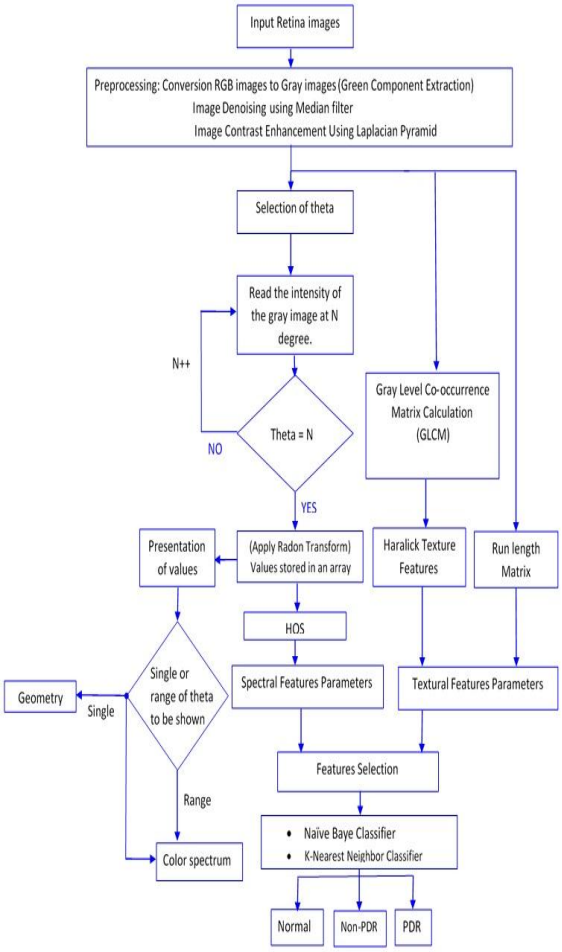

Fig 2. Proposed Methodology Flow chart

a. Preprocessing of Image Data

Feature extraction is most important part in this project and is widely used in classification processes. This extraction is carried out after preprocessing the images. It is thus necessary to resize retina images convers it to gray, Denise images and improve the contrast of the image, which will result in better feature extraction process. Figure 3, shows the pre-processing step primarily consists of resizing image to 512×512, then the green component is extracted and introduced to the Median Filter The median filter is a non-linear filter type and which is used to reduce the effect of noise without blurring the sharp edge. The operation of the median filter is – first arrange the pixel values in either the ascending or descending order and then compute the median value of the neighborhood pixels. Laplacian pyramid has been used for image enhancement so as to obtain an output image persisting its naturalness with an improved local and global contrast. Laplacian pyramid is used for separating the brightness and contrast components of an image. The brightness component is characterized by slow spatial variations and contrast components tend to vary abruptly. Therefore, the brightness component has low frequency while the contrast component tends to have a relatively

high frequency. Each band of Laplacian pyramid [14][15] is the difference between two adjacent low-pass images of the Gaussian pyramid $[I_0, I_1 \dots I_N]$. Image enhancement is an important step in preprocessing stage. The objective of image enhancement is to increase the visual perception of the image o that they are more suitable for human viewers or machine vision applications. It is well known in the image processing society that there is no unifying or general theory for image enhancement algorithms. Thus an enhancement algorithm that is suitable for some application may not work in other applications. In image processing technology, image enhancement means improving image quality through a broad range of techniques such as contrast enhancement, color enhancement, dynamic range expansion, edge emphasis, and so on.

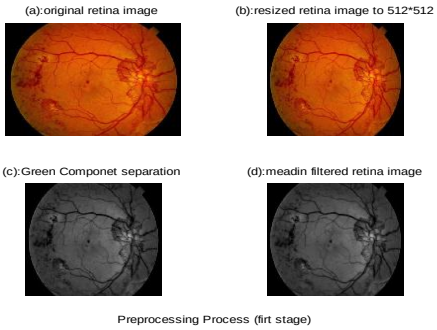

Fig 3. Steps to the image pre-processing

Thus image enhancement based on Laplacian Pyramid (LP) starts by the Generation of Laplacian Pyramid for the given image, for n particular levels. Figure 4 shows Laplacian Image decompositions for retina image. So following is the reconstruction equation

$$I_0 = I_N + \sum_{n=1}^{N} D_n \quad \dots (1)$$

Where N is the decomposition layer. This phase involves pyramid expansion and then its reduction. Pyramid expansion for an image of size m by n will create a result of size $(2m-1)$ by $(2n-1)$. Pyramid reduction would cause an image of size m by n to produce a result of size ceil $(m/2)$ by ceil $(n/2)$.

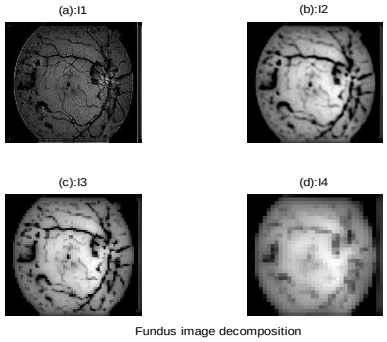

Fig 4.Fundus image pyramid decomposition

b. Laplacian Contrast Enhancement

The image enhancement technique employed by joint effort of histogram equalization and Laplacian pyramid aims to overcome the quantum jump that conventional histogram equalization based algorithms are likely to suffer from and for supplementing the improved local details that those methods cannot provide due to their inherent limitations. The proposed combination framework aims to provide an output image with well natural look without over-enhancement or severe failure and this very important to preserve the tiny areas in retina images. Contrast enhancement [16][17] improves the perceptibility o objects in the scene of enhancing the brightness difference between the objects and their backgrounds. Here the laplacian method has been used for improving contrast of an image. The histogram with gray levels in the range K $[0, L-1]$ is a discrete function as $h(I_k) = n_k$ where I_k is the k[th] gray level in K and n_k represents the number of pixels having gray levelI_k. In the histogram, a ridge shape with some consecutive luminance levels can be regarded as the feature area of an image. To globally distinguish between ridges and valleys and remove their ripples, we smooth the histogram [18][19][20] like as follows:

$$hg(I_k) = h(I_k).g(I_k) \qquad \dots(2)$$

$g(x) = -e^{x^2}$ Where $g(x)$ is a Gaussian function, *x* is the corresponding location to a bin of the histogram, and coefficients of the Gaussian filter are normalized. Boosting minor areas which are a key strategy of proposed contrast enhancement to suppress quantum jump. First, the peak value in the smoothed histogram$hg(I_k)$ is found as:

$P(K) = \max_{k \in K}\{hg(I_k)\}$ ...(3)

Second, the ridges between valleys are searched and boosted. Ridge boundary is defined as the bins between the first point of the positive slope and the last point of the negative slope. The constant factor of enhancement and then the local minor areas of histogram have to be found. The local maxima have been checked, if it is found it means a peak value is found and then need to enhance it and store value to new histogram. Then Slantwise clipping stage then is started the clipping technique is used as it effectively suppresses for the quantum jump. The mean of newly generated histogram and then the mid value have been determined and then the residual from local and global clipping are gathered. Then the stage of new image generation is started, which involve finding the normalized cumulative histogram:

$$h = 255\left[cdf - \frac{cdf(min)}{MN} - cdf(min)\right] \quad \dots(4)$$

Finally replace old histogram with new equalized values. Figure 5 below shows the output of proposed enhancement technique on retina image

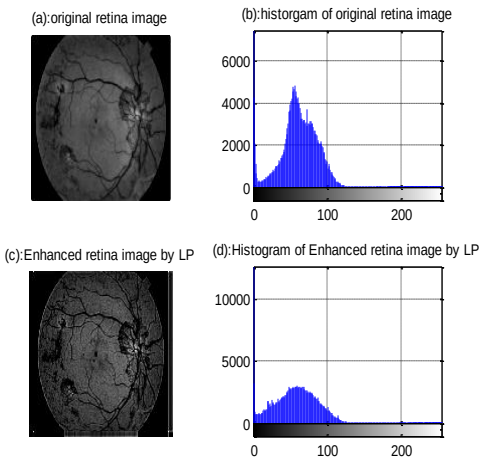

Fig5. Output of proposed enhancement technique on retina image

c. Radon Transform

Radon Transform is the projection of an image matrix along specified directions which extract features from the image. The radon function computes the line integrals which cut across the origin at specified angles from multiple sources along parallel paths. Each beam is 1-pixel unit apart. To convert a two-dimensional image to one-dimensional image, the radon function takes multiple, parallel-beam projections of the image from different angles by rotating the source around the center of the image. Theta is set to 0:179 where the range of projection is between zero and 179 degrees in the anti-clockwise direction. The step projection increment is default at one degree where it takes the features from the image at each and every one degree from zero to 179 degree. The below figure explains how radon transform works. The transform function is given in equation blow:

$$R(\rho.\theta) = \int u(\rho cos\theta - Ssin\theta, \rho sin\theta + Scos\theta)ds \quad \dots(5)$$

Where the function $R(\rho,\theta)$ is called the Radon transform of the function $u(x,y)$.This equation describes the integral along the line, s, through the image, where ρ is the distance of the line integral from the origin and theta, θ, is the angle from the horizontal [21][22]. The integral line extracts the features of the image where it converts the intensity of the image into values. Brighter part of the image will have a higher value while darker part of the image will have a lower value

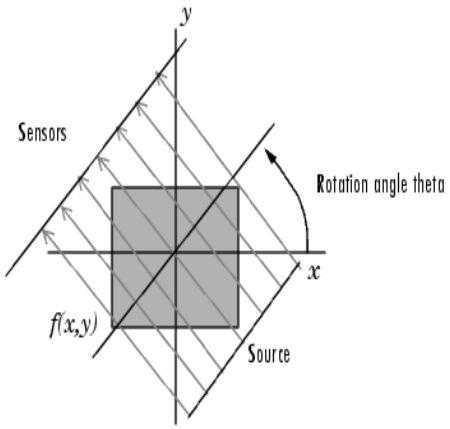

Fig 6. Projection of Radon Transform

. The integral line will shift towards the origin when ρ is reduced and it can be shifted until negative p values. It will take the reading at every ρ value.

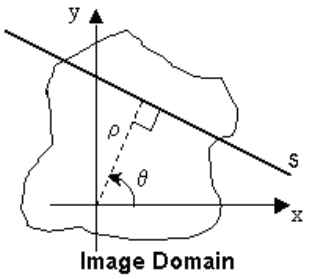

Fig7. Image domain of Radon Transform

The range of the ρ values can be specified by the programmer. To take the reading from another angle, the theta will change and it applies the above steps again. Moreover, it will sum up the reading values for each S value. The interception point between ρ and s is the origin of the integral line where the equation takes the reading from negative to positive infinite.

III. FEATURE EXTRACTION

Feature extraction is the process of obtaining higher level information of an image such as color, shape and texture. Spectral and textual are two fundamental pattern elements that are interpreted by human. The features vector. The feature vector used for classification consists initially of twenty-six features. These features are Homogeneity, Energy, Entropy Contrast, Symmetry, Correlation, and Momentum1, Momentum2, Momentum3, Momentum4 Angular 2nd Momentum Difference, Contrast Difference, Mean Difference, Entropy Difference, Short Run Emphasis, Long Run Emphasis, Run Percentage, Gray Level Non Uniformity and , Run Length Non Uniformity .while the spectral features are ,normalized bispectral entropy1 ,normalized bispectral ent2, normalized bispectral entropy3 ,bispectrum phase entropy, mean bispectrum magnitude.

a. Higher Order Spectra Features

Studies have shown that the "shape" of a signal is a function of its phase signals with different wave shape and may have the same power spectrum. Assuming that there is no bi-spectral aliasing, the bi-spectrum of a real signal is uniquely defined with the triangle [23]. Parameters are obtained by integrating along the straight lines passing through the origin in bi-frequency space. The region of computation and the line of integration are depicted in Figure 8. The bi-spectral invariant, p (a), is the phase of the integrated bi-spectrum along the radial line with the slope equal to a.

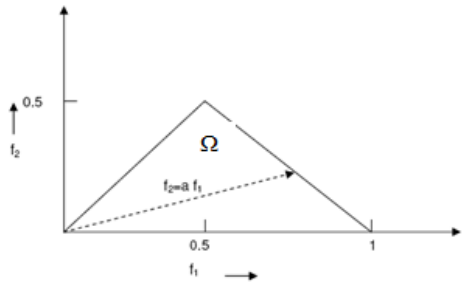

Figure 8: The Bi-spectrum curve

This is defined by:

$$p(a) = \arctan\left(\frac{I_i(a)}{I_r(a)}\right) \quad \dots(6)$$

Where

$$I(a) = \int_{f_{1=0^+}}^{\frac{1}{1+a}} B(f_1, af_1)\, df_1 = I_r\,(a) + jI_i(a) \quad \dots(7)$$

For $0 < a \leq 1$, and $j = \sqrt{-1}$. The variables $I_r$and I_i refer to the real and imaginary part of the integrated Bi-spectrum respectively. In this work, the one dimensional Radon transformed fundus images are analyzed using different higher order spectra (also known as polyspectra) that are spectral representations of higher order moments or cumulate of a signal. In particular, this paper studies features related to the third order statistics of the signal, namely the bispectrum. The Bispectrum is the Fourier transform of the third order correlation of the signal and is given by:

$$B(f_1, f_2) = E[X(f_1).X(f_2).X^*(f_1 + f_2)] \dots(8)$$

Where $X(f)$ is the Fourier transform of the signal $x(nT)$ and $E[.]$ stands for the expectation operation. In practice, the expectation operation is replaced by an estimate that is an average over an ensemble of realizations of a random signal. For deterministic signals, the relationship holds without an expectation operation with the third order correlation being time-average. For deterministic sampled signals, $X(f)$ is the discrete-time Fourier transform (DFT) and in practice is computed at frequency samples using the fast Fourier transform (FFT algorithm). The frequency f may be normalized by the Nyquist frequency to be between 0

and 1. The bispectrum is a complex-valued function of two frequencies. The magnitude of the bispectrum may be normalized (by power spectra at component frequencies) such that it has a value between 0 and 1, and indicates the degree of phase coupling between frequency components [24]. In this study normalized bispectrum by Haubrich [25] was used to analyze the fundus images after convert them to the frequency domain by using Radon transform. Its formula is given by:

$$B_{norm}(f_1, f_2) = \frac{E[X(f_1).X(f_2).X^*(f_1+f_2)]}{\sqrt{p(f_1).p(f_2).p(f_1+f_2)}} \quad \dots(9)$$

Where $p(f)$ is the power spectrum Bicoherence $B_{co}(f_1, f_2)$, is defined as the squared magnitude of the above normalized bispectrum. In order to differentiate the characteristics of fundus images a set of features have been derived. These features are the mean magnitude and the phase entropy. The features are calculated within the region defined in figure 8. The formulae of these features are:

$$M_{ave} = \frac{1}{L}\sum_{\Omega} B_{norm}(f_1, f_2) \quad \dots(10)$$

$$P_e = \sum_{n} p(\psi_n).log\big(p(\psi_n)\big) \quad \dots(11)$$

$$\psi_n = \left\{\phi \setminus -\pi + \frac{2\pi n}{N} \le \phi < -\pi + \frac{2\pi(n+1)}{N}, \qquad n = 0,1,\dots,N-1\right\}$$

$$p(\psi_n) = \frac{1}{L}\sum_{\Omega} I\big[\phi\big(B_{norm}(f_1, f_2)\big) \in \psi_n\big] \quad \dots(12)$$

L is the no of point within the region Ω in figure 8, ϕ Refers to the phase angle of the bispectrum, $I(.)$ = indicator function. The bi-spectral phase is quantized and a histogram is computed as an estimate of the probability density function of the phase. The entropy used is the Shannon entropy. The mean magnitude of the bispectrum can be useful in discriminating between processes with similar power spectra but different third order statistics. However, it is sensitive to amplitude changes. Normalization can easily take care of such variation. The phase entropy would be zero if the process were harmonic and perfectly periodic and predictable. As the process becomes more random, the entropy increases. Unlike, Fourier phase, the bi-spectral phase does not change with a time shift in this work, in our attempt to characterize the regularity or irregularity of the Radon transformed retina images which contain or not the symptoms of diabetic retinopathy from bispectrum plots, two additional bi-spectral entropies similar to that of Spectral entropy. The formulae for these bi-spectral entropies are given as:

Normalized Bi-spectral Entropy (BE1):

$$p_1 = -\sum_n p_n . \log(p_n) \quad \ldots (13)$$

Where

$$p_n = \frac{|B_{norm}(f_1, f_2)|}{\sum_\Omega |B_{norm}(f_1, f_2)|} \quad \ldots (14)$$

Normalized Bi-spectral Squared Entropy (BE2):

$$p_2 = -\sum_i p_i . \log(p_i) \quad \ldots (15)$$

Where

$$p_i = \frac{|B_{norm}(f_1, f_2)|^2}{\sum_\Omega |B_{norm}(f_1, f_2)|^2} \quad \ldots (16)$$

Normalized Bispectrum Cubed Entropy (BE3)

$$p_3 = -\sum_j p_j . \log(p_j) \quad \ldots (17)$$

where

$$p_j = \frac{|B_{norm}(f_1, f_2)|^3}{\sum_\Omega |B_{norm}(f_1, f_2)|^3} \quad \ldots (18)$$

The normalization in the equations above ensures that entropy is calculated for a parameter that lies between 0 and 1 (as required of a probability) and hence the entropies $p_1, p_2,$ and p_3 computed are also between 0 and 1.

b. Textural Features

The presented features were derived from Gray Level Co-occurrence Matrix and run length matrix. Hence Haralick introduced Gray Level Co-occurrence Matrix and texture features [28]. It consists of two steps for feature extraction. First is to compute the co-occurrence matrix and second step is to calculate texture features based on the co –occurrence matrix. This technique has been widely used in image analysis applications especially in the biomedical field. Gray Level Co-occurrence Matrix for an image of size $M \times N$, the gray level co-occurrence matrix (GLCM) is defined as:

$$C_d(i,j) = |\{(p,q),(p+\Delta x, q+\Delta y); I(p,q) = i, I(p+\Delta x, q+\Delta y) = j\}| \quad \ldots (19)$$

Where $(p,q),(p+\Delta x, q+\Delta y) \in M \times N$, $d = (\Delta x, \Delta y)$ and $|.|$ denotes the cardinality of a set. Given a grey level i in an image, the probability that the gray level of a pixel at a $(\Delta x, \Delta y)$ distance away j is:

$$p_d(i,j) = \frac{C_d(i,j)}{\sum C_d(i,j)} \quad \ldots (20)$$

In this work, eleven Haralick Texture Features were derived from the gray level matrix for an image. The following features were selected. Contrast is the measurement of the local variations or differences in the

GLCM. It works by measuring how elements do not lie on the main diagonal and returns a measure of the intensity contrast between a pixel and the neighboring pixels over the whole image. Large contrast reflects large intensity difference in GLCM.

$$contrast = \sum_i \sum_j (i-j)^2 \, p_d(i,j) \quad \dots(21)$$

Homogeneity measures how close the distribution of elements in the GLCM is to the diagonal of GLCM. Homogeneity weighs values by the inverse of the contrast weight, with weights decreasing exponentially away from the diagonal as shown in equation (21). The addition of value '1' in the denominator is to prevent the value '0' during division. As homogeneity increases, the contrast typically decreases.

$$Homogeneity = \sum_i \sum_j \frac{1}{1+(i-j)^2} p_d(i,j) \quad \dots(22)$$

Entropy is understood from the concept of thermodynamics. It is the randomness or the degree of disorder present in the image. The value of entropy is the largest when all elements of the co-occurrence matrix are the same and small when elements are unequal.

Energy is sometimes derived from the use of angular second moment. It is the sum of squared elements in the GLCM known as angular second moment

$$Entropy = -\sum_i \sum_j p_d(i,j).ln\big(p_d(i,j)\big) \quad \dots(23)$$

$$Entropy = \sqrt{Angular\ 2^{nd} Momentum} \quad \dots(24)$$

And

$$Angular\ 2^{nd} Momentum = \sum_i \sum_j \big(p_d(i,j)\big)^2 \quad \dots(25)$$

Basically, it is the measurement of the denseness or order in the image. Moments 1 to 4 are defined as:

$$m_g = \sum_i \sum_j (i,j)^g \left(p_d(i,j)\right) \quad \dots(26)$$

Where g is the integer power exponent that defines the moment order. Moments are the statistical expectation of certain power functions of a random variable and are characterized as follows: moment 1 is the mean which is the average of pixel values in an image; moment 2 is the standard deviation; moment 3 measures the degree of asymmetry in the distribution; and moment 4 measures the relative peak or flatness of a distribution and is also known as kurtosis. Difference Statistics are defined as the distribution of probability $p_\delta(k);\ k = 0, \dots, n-1$, and k is gray level difference between the points separated by δ in an image.

They are a subset of co-occurrence matrix and the distribution of probability $p_\delta(k)$ is defined as:

$$p_\delta(k) = \sum_i \sum_j C_d(i,j) \quad \dots(27)$$

Hence the Angular second momentum (ASM) is calculated as:

$$ASM = \sum_{k=0}^{n-1} \left(p_\delta(k)\right)^2 \quad \dots \quad (28)$$

When the $p_\delta(k)$ values are very similar or close, ASM is small. ASM is large when certain values are high and others are low. Contrast is also known as the second moment of $p_\delta(k)$ (its moment of inertia about the origin).

$$contrast = \sum_{k=0}^{n-1} k^2\, p_\delta(k) \quad \dots \quad (29)$$

When $p_\delta(k)$ values are concentrated near the origin, mean is small and mean is large when they are far from the origin.

$$Mean = \sum_{k=0}^{n-1} k\, p_\delta(k) \quad \dots \quad (30)$$

Entropy is smallest when $p_\delta(k)$ values are unequal, and largest when $p_\delta(k)$ values are equal. Entropy is directly proportional to unpredictability. The above-mentioned features were calculated for $\delta = (0,1),(1,1),(1,0)$, and the total mean values on the four features were taken.

$$Entropy = -\sum_k p_\delta(k)\,.\,log p_\delta(k) \quad \dots(31)$$

Run-length statistics capture the coarseness of a texture in specified directions. A run is defined as a string of consecutive pixels which have the same intensity along a specific linear orientation. Fine textures tend to contain more short runs with similar intensities, while coarse textures have more long runs with significantly different intensities. Run length matrix, $p_\theta(i,j)$ records the frequency that j points with a gray level i continue in the direction θ. The i^{th} dimension of the matrix corresponds to the gray level and has a length equal to the maximum gray level, n, while j^{th} corresponds to the run length and has length equal to the maximum run length, l. Five measures from run-length matrixes of θ = 0̊, 45̊, 90̊, and 135̊ were computed by as follows.

$$Short\ Run\ Emphasis = \frac{\sum_i \sum_j p_\theta(i,j)/j^2}{\sum_i \sum_j p_\theta(i,j)} \qquad \dots(32)$$

Short run lengths are emphasized by dividing each run length value by the square of its length. The total number of runs in the image is the

denominator.

$$Long\ Run\ Emphasis = \frac{\sum_i \sum_j j^2 p_\theta(i,j)}{\sum_i \sum_j p_\theta(i,j)} \qquad \dots(33)$$

In order to allow higher weight to the long runs, each run length value is multiplied by the square of its length.

$$Run\ Percentage = \frac{\sum_i \sum_j p_\theta(i,j)}{A} \quad \dots(34)$$

Where A is the area of the image. This particular feature is the ratio between the total number of observed runs in image and the total number of possible runs if all runs had a length of one.

$$Gray\ Level\ Non-Uniformity = \frac{\sum_i \{\sum_j P_\theta(i,j)\}}{\sum_i \sum_j p_\theta(i,j)} \qquad \dots(35)$$

This feature depends on high run length values. The gray level non-uniformity feature will have its lowest value if the runs are evenly distributed over all gray levels.

$$Run\ Length\ Non-Uniformity = \frac{\sum_i \{\sum_j P_\theta(i,j)\}}{\sum_i \sum_j p_\theta(i,j)} \qquad \dots(36)$$

IV. CLASSIFICATION:

Classes based on the features the samples carry. In this project, Naïve Baye and K-nearest neighbor classifier have been employed. 150 fundus images which consist of 50 Normal fundus images and 50 Non proliferative diabetic retinopathy and 50 image Proliferative diabetic retinopathy were used. The database used in this work is publicly available database called MESSIDOR. The MESSIDOR dataset which is composed of 1200 color fundus images acquired using a variety of retina-graphs. The image resolution is comprised between 870 pixels and 1400 pixels. All retina images have been resized to 512 pixels *512 pixels. Three different ratios are used during the training of classifiers which all depicted in Table 1

Table 1: Training Set and Ratio for testing and training

First Training	30% Training	70% Testing
Second Training	70% Training	30% Testing
Third Training	30% Training (Random)	70% Testing

The different classes for output and training are represented as numbers shown in the table 2 below:

Table 2: Class Labels

Classes	Number
Normal	1
Non-PDR	2
PDR	3

V.EXPERIMENTAL AND SIMULATION RESULTS

Out of 26 features retrieved with the proposed technique (Spectral-Textural), 10 features were selected using p-value which is the probability of rejecting the null hypothesis assuming that the null hypothesis is true. The p-value has been calculated for all presented features are subjected to the ANOVA (Analysis Of Variance between groups) test to obtain the 'p-value'. ANOVA uses variances to decide whether the means are different. Then input features of retina images have been fed into the proposed classifiers (naïve Bayes and K-Nearest Neighbor). This test uses the variation (variance) within the groups and translates into variation (i.e. differences) between the groups, taking into account how many subjects there are in the groups. If the observed differences are high, then it is considered to be statistical significant. For spectral feature based system which involves (normalized bi-spectral entropy1, normalized bi-spectral ent2, normalized bi-spectral entropy3, bispectrum phase entropy, mean bispectrum magnitude), 50 bi-spectrum invariants feature values were extracted for each retina image by allowing the Radon Transform orientation angle change from 0^o to 80^o with step of 20^o. Initially Out of the 50 bi-spectrum features. Basically the lowest 'p-value' 7 features were selected. The same criteria have been applied on the textural parameters features, hence 19 features using gray level co-occurrence matrix of 135^o and Run Length Matrix at also 135^o were selected out of 152 features (19 textures parameters by 8 angles started from 0^o to 360^o step 45^o), finally, from the last 26 features the best 12 were selected which have p-value less than or equal to 0.001. Figure (9) depicts graphical illustration for the nominated features with their p-value. The feature vector consists the following features [Entropy-(2), Contrast-(3), Momentum1(4), Momentum4(7), Mean difference (10), Entropy difference (13), Run Percentage (14), Gray Level Non-Uniformity (17), Normalized bi-spectral (18) ent2-80(21), bispectrum (23) phase ent-0(25)]. The reasons for the p-value to be very small in these seven features could be that at this parameter, there are obvious blood vessels, hemorrhages or micro aneurysms to distinguish the difference between the three groups. Figures (10) and (11) depict a graphical illustration for two out of ten features employed in feature vector.

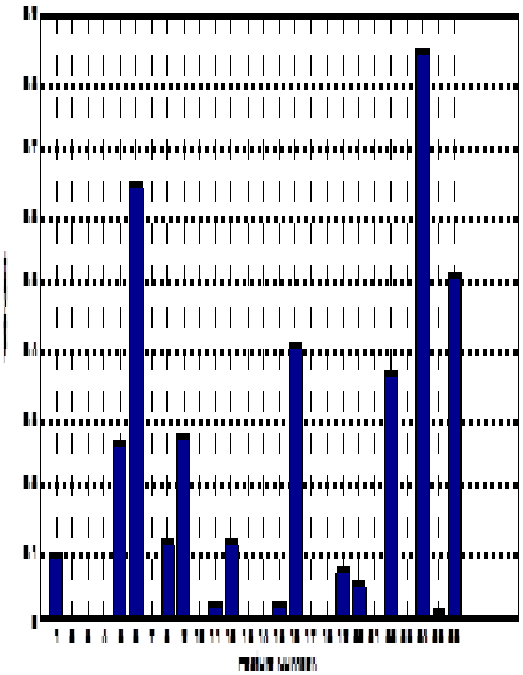

Fig 9. Depicts graphical illustration for the nominated features with their p-value

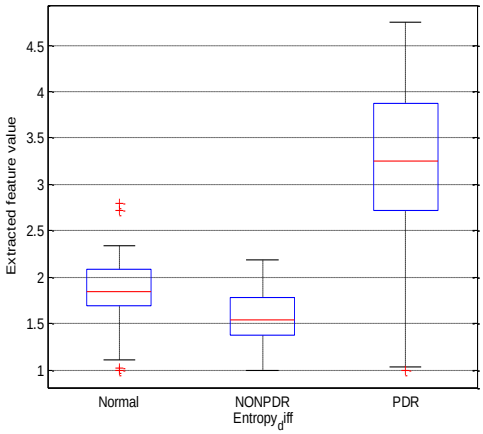

Fig10. Normalized values for the Difference Entropy feature for the three categories (Normal, Non-PDR, and PDR)

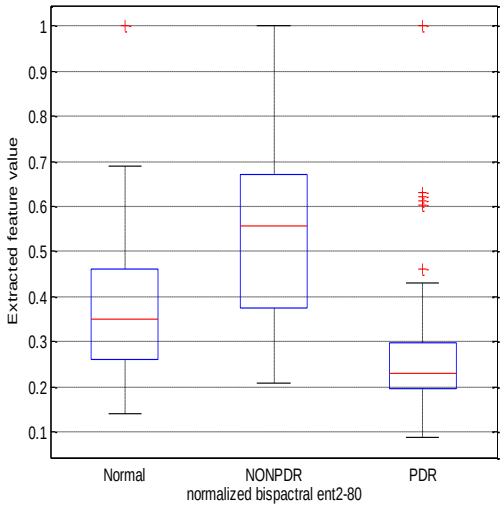

Fig11. Values for the normalized bi-spectral entropy 2 at angel theta of 80o feature for the three categories (Normal, Non-PDR, and PDR)

From Figures12, to 17 (for the training and testing files depicted in table 1) it is observed that classification using all the ten features (Spectral-Textural) features, by the Naïve Baye yields the highest classification accuracy as compared to K-nearest neighbor classifier even the fact that the proposed new technique which is a mixture between spectral and textural technique give high classification accuracy.

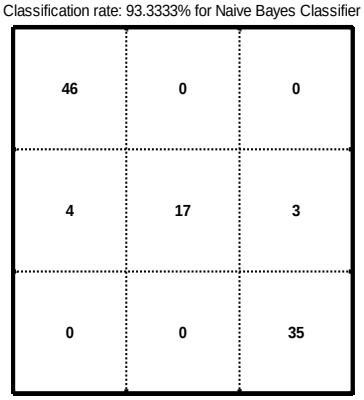

Fig 12.The resulted confusion matrix and Classification rate for first training using Naive Bayes Classifier

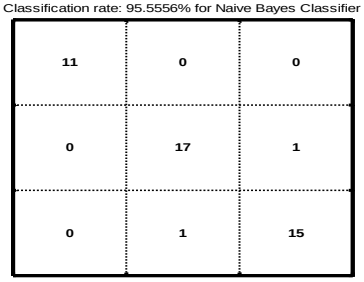

Fig13.The resulted confusion matrix and Classification rate for second training using Naive Bayes Classifier

Classification rate: 96.1905% for Naive Bayes Classifier

20	0	0
2	12	2
0	0	69

Fig14.The resulted confusion matrix and Classification rate for third training using Naive Bayes Classifier

Classification rate: 96.1905% for KNN Classifier

30	0	0
0	37	2
0	2	34

Fig15.The resulted confusion matrix and Classification rate for first training using KNN-Classifier

Classification rate: 95.5556% for KNN Classifier

11	0	0
0	19	2
0	0	13

Fig16.The resulted confusion matrix and Classification rate for second training using KNN-Classifier

Classification rate: 98.0952% for KNN Classifier

41	0	0
0	11	2
0	0	51

Fig17.The resulted confusion matrix and Classification rate for third training using KNN-Classifier

From Figures 12-16, it is observed that the best results for MESSIDOR database (98.095%), whereas the average was (96.6%) classification accuracy has been obtained for retina images classified with KNN classifier while using naive Bayes classifier result on an average accuracy of 97%. Thus the abnormality detection is done with higher accuracy.

VI. CONCLUSION

In this work, the KNN and Naive Bayes classifiers are trained through supervised learning for the features extracted to classify the retinal images. The retinal images used in this work are obtained from the publicly available MESSIDOR databases. There are two modules in this work, one that extract the image features using radon transform and one use statistical features the comprehensive features were filtered and only 10 features had been used by the proposed system The best classification accuracy obtained is 98.09%. The developed system will provide a second opinion to the ophthalmologist to do accurate diagnosis.

REFERENCES

[1] SALZ, D. A. & WITKIN, A. J. (2015). "Imaging in Diabetic Retinopathy". *Middle East African journal of ophthalmology*, 22, p145.

[2] SKAGGS, J. B., ZHANG, X., OLSON, D. J., GARG, S. & DAVIS, R. M. (2017). "Screening for Diabetic Retinopathy Strategies for Improving Patient Follow-upC". *North Carolina medical journal*, 78, p121-123.

[3] Vishali Gupta,etal, (2007) *Diabetic Retinopathy Atlas and Text*. 1st edition, Jaypee Brothers Medical Publications.

[4] Bazhdar N. SH. Mohammed, Raghad Z. Yousif (2019). *Intelligent System for Screening Diabetic Retinopathy by Using Neutrosophic and Statistical Fundus Image Features*. ZANCO Journal of Pure and Applied Sciences The official scientific journal of Salahaddin University-Erbil, ISSN (print):2218-0230, ISSN (online): 2412-3986, DOI: http://dx.doi.org/10.21271/zjpas.

[5] Vijay M. Mane, Dattatray V. Jadhav, (2014). "Progress towards Automated Early Stage Detection of Diabetic Retinopathy: Image Analysis Systems and Potential", *Journal of Medical and Biological Engineering*, 34(6): p520-527.

[6] Giri Babu Kande, April, 2010. "Feature Extraction from Fundus Images to Analyze Diabetic Retinopathy. Research and Development Cell" *Jawaharlal Nehru Technological University Hyderabad Kukatpally, Hyderabad* – 500 085, India.

[7] A.M. Mendonça et al. (27 Sep 1999). "Automatic segmentation of microaneurysms in retinal angiograms of diabetic patients". *IEEE International Conference on Image Analysis and Processing.*

[8] Abhir Bhalerao et al. (2008). "Robust Detection of Microaneurysms for Sight Threatening Retinopathy Screening". *IEEE Computer society*.
[9] Iqbal, M.I et al. (2006). "Automatic Diagnosis of Diabetic Retinopathy using Fundus images", *Blekinge Institute of Technology*.
[10] Akara Sopharak et al. (2011). "AutomaticMicroaneurysm Detection from None dilated Diabetic Retinopathy Retinal Images Using Mathematical using Morphology methods" *IAENG International journal of computer science.*
[11] Priya. R et al. (2011). "Review of automated diagnosis of diabetic retinopathy using the support Vector machine", *International Journal of Applied Engineering Research, Dindigul*, Volume 1, No 4.
[12] S.Saranya Rubini, etal, (2015) "diabetic retinopathy detection Based of Eigenvalues of the Hessian matrix", *Elsevier Procedia Computer sciences* ,47 ,p 311-318.
[13] Vijay M Mane etal, (2015) "Detection of Red Lesions in Diabetic Retinopathy Affected Fundus Images", *IEEE International Advance Computing Conference (IACC)*
[14] Mahendran Gandhi,etal, (2015) "Investigation of Severity of Diabetic Retinopathy by detecting Exudates with respect to Macula" This full-text paper was peer-reviewed and accepted to be presented at the *IEEE ICCSP conference.*
[15] P. J. Burt, and E. H. Adelson, (1983). "The Laplacian Pyramid as a Compact Image Code," *IEEE Trans. Commun.*, vol. 31, no. 4, pp. 532-540.
[16] S. M. Pizer, E. P. Amburn, J. D. Austin, R. Cromartie, A. Geselowitz etal., (Sep, 1987). "Adaptive Histogram Equalization and Its Variations," *Computer Vision Graphics and Image Processing*, vol. 39, no. 3, pp. 355-368.
[17] J. Y. Kim, L. S. Kim, and S. H. Hwang, (Apr, 2001) "An advanced contrast enhancement using partially overlapped sub-block histogram equalization," *IEEE Transactions on Circuits and Systems for Video Technology*, vol. 11, no. 4, pp. 475-484.
[18] K. Tae Keun, P. Joon Ki, and K. Bong Soon, (1998). "Contrast enhancement system using spatially adaptive histogram equalization with temporal filtering," *IEEE Trans. Consume. Electron.* vol. 44, no. 1, pp. 82-87.
[19] T. Arici, S. Dikbas, and Y. Altunbasak, (2009). "A Histogram Modification Framework and Its Application for Image Contrast Enhancement," *IEEE Trans. Image Process.*, vol. 18, no. 9, pp. 1921-1935.
[20] S. S. Agaian, B. Silver, and K. A. Panetta, (2007). "Transform Coefficient Histogram-Based Image Enhancement Algorithms Using

Contrast Entropy," *IEEE Trans. Image Process*. vol. 16, no. 3, pp. 741-758.
[21] S. Chandra and I. Svalbe, (2009)."A fast number theoretic finite Radon transform," *Digital Image Computing: Techniques and Applications,* pp. 361–368.
[22] V. Venkatraghavan, S. Rekha, J. Chatterjee, and A. K. Ray, "Modified Radon transform for texture analysis," no. 2, pp. 9–12.
[23] B. Kaur and M. K. Majumder, (March 2012) "Novel VLSI architecture for two-dimensional Radon transform computations," *1st International Conference on Recent Advances in Information Technology*, pp. 570–575.
[24] Nikias, C.L., Petropulu, A.P., (1993) *Higher-order spectra analysis: a nonlinear signal processing framework*, Englewood Cliffs, N.J.: PTR Prentice Hall,.
[25] Cesar Seijas, Antonino Caralli, Sergio Villazana, (2013). Neuropathology Classifier Based on Higher Order Spectra", *Journal of Computer and Communications*, 1, 28-32.